Numerical Investigation of Non-Newtonian Casson Fluid Flow with Radiative Heat Transfer Over a Magnetized Stretching Surface.

Golbert Aloliga[1*], Christian John Etwire[2], Isaac Azure[3], Enoch Deyaka Mwini[4]

[1]Department of Mathematics/ICT St. Vincent College of Education, P.O. Box YD 184, Yendi, Northern Region, Ghana.

[2]C. K. Tedam University of Technology and Applied Sciences, P.O. Box 24, Navrongo, Ghana

[3]Department of Mathematics, Kwame Nkrumah University of Science and Technology, Kumasi, Ghana

[4]Department of Mathematics/ICT, Tamale College of Education, Tamale-Ghana

[*]Corresponding Author

DOI: https://doi.org/10.51584/IJRIAS.2026.110100120

Received: 03 February 2026; Accepted: 09 February 2026; Published: 19 February 2026

ABSTRACT

A comprehensive study has been conducted on the numerical investigation of non-Newtonian Casson fluid flow with radiative heat transfer over a magnetized stretching surface. The study considers the influence of surface magnetization, thermal radiation, convection, and temperature fields. The study considers the influence of surface magnetization, thermal radiation, convection, and temperature fields. A novel modification to the Casson fluid model has been introduced by altering its order. Using a similarity approach, the governing equations are transformed into ordinary differential equations. The parameters governing the flow are analysed numerically. The effects of surface magnetization on the flow of this modified fluid are presented in tabular form. It is found that surface magnetization increases the thickness of the thermal boundary layer, thereby significantly enhancing heat transfer control. The magnetized surface also impacts skin friction, Nusselt number, and Sherwood number similarly. This study suggests the potential benefits of incorporating magnetized surfaces in fluid flow applications for efficient flow control, as well as the advantages of adjusting the Casson fluid order.

Keywords: Casson order, Casson parameter, internal heat generation, convection term, and thermal diffusivity.

INTRODUCTION

This review synthesizes recent developments in the dynamics of Casson fluids over stretching sheets, with a specific focus on the transition from external magnetic fields (MHD) to intrinsic surface magnetization. While standard MHD flows are well documented, they typically exert a retarding Lorentz force. The emergence of magnetized surfaces fills a critical gap by generating wall-parallel Lorentz forces that assist rather than retard flow. The Casson fluid, introduced by Casson (1959), is a classical fluid model with significant relevance to industrial applications. The complex rheological behaviour of the Casson fluid, characterized by both linear and nonlinear structures, has recently garnered increased attention due to its valuable applications and importance across a variety of industries. Since its development, this fluid has been recognized as one of the best of its kind. The Casson fluid is a shear-thinning liquid that is assumed to exhibit infinite viscosity at zero shear rate and zero viscosity at infinite shear rate, with a yield stress below which no flow occurs (Dash et al., 1996). Advances in science and technology have prompted researchers to explore various methods for optimizing heat transfer during the cooling of industrial products to achieve desired properties. Heat transfer in non-Newtonian fluids plays a crucial role in numerous industrial applications and is integral to modern industrial processes, where these fluids serve as media for heat transport. Non-Newtonian fluids, such as honey, blood, grease, and oil, are classified into various types, including Jeffrey fluids, Maxwell fluids, second- and third-grade fluids, Casson fluids, and viscoelastic fluids (Aliseda et al., 2008). These fluids have numerous technological applications, such as in the cooling processes of microchips, solar energy recovery, open-flow switching, and simulations of reservoirs and nuclear reactors. Casson fluid, a specific type of non-Newtonian fluid, has been characterized by

ISSN No. 2454-6194 | DOI: 10.51584/IJRIAS |Volume XI Issue I January 2026

Xiong et al. (2008) as a shear-thinning liquid exhibiting yield stress at zero shear rates. They noted that viscosity is a crucial property that governs the thinning and thickening of the boundary layer. Due to its nonlinearity and complex nature, a single constitutive relation cannot fully describe the rheological properties of Casson fluids. As a result, numerous studies have examined this model under various rheological conditions. Many engineering processes involve high temperatures and radiative environments, which are critical in the design of relevant equipment (Seddeek, 2001). Research on steady magnetohydrodynamic (MHD) flow over different surfaces has been reported by Makinde (2001) and Makinde and Ogulu (2008). A notable application of MHD is in the cooling of nuclear reactors using liquid sodium. Radiation effects on chemically reacting boundary layer flow with MHD are present in many practical heat transfer situations (Ibrahim and Makinde, 2011). Additionally, convective flows of non-Newtonian fluids play a crucial role in agriculture, particularly in the exploration of sub-ground water reservoirs (Sharmila and Kaleeswari, 2015). Arthur et al. (2015) employed similarity analysis to study the flow of Casson fluid over a vertical porous surface with chemical reactions in the presence of a transverse magnetic field. They observed a decrease in both velocity and temperature as the magnetic and Casson parameters increased. Mustafa et al. (2011) investigated the unsteady boundary layer flow and heat transfer of a Casson fluid over a moving flat plate with a parallel free stream using the Homotopy Analysis Method (HAM). El-Aziz and Afify (2016) studied the MHD flow of a Casson liquid film with variable thermal conductivity and thermal radiation. The growing application of non-Newtonian Casson fluids has spurred further research into the behaviour of Casson-type nanofluids, as noted by Ishak et al. (2010).

Recent studies have extensively explored MHD flows influenced by thermal effects and chemical reactions in porous media. Chenna et al. (2025) examined chemical processes and Soret effects on MHD free convection along an accelerated vertical plate through a porous medium with a heat source. Their findings highlight the significance of thermal diffusion in isotope separation, especially in gas mixtures with light molecules like helium and hydrogen. Yahaya and Faisal (2018) studied temperature stratification in MHD nanofluid radiative flow over nonlinear stretching sheets, noting improvements in temperature, velocity, and nanoparticle concentration. Chenna et al. (2023) focused on chemical reactions affecting MHD-Casson nanofluid flow over a porous stretched sheet with suction or injection, enhancing understanding of how chemical processes and magnetic fields influence non-Newtonian fluids. Significant contributions also include Gireesha et al. (2019), who analyzed Ohmic heating in Casson fluid MHD mixed convection flow; Gbadeyan (2018), who explored Dufour and Soret effects on mass and heat transfer, finding wave-like patterns along the y-axis; and Oreyeni and Omokhuale (2019), who used the Homotopy analysis method to examine these effects in MHD natural convection with thermal stratification. Rasool et al. (2020) investigated the roles of Soret and Dufour numbers on binary chemical reactions and thermal radiation in Darcy-Forchheimer nanofluid flow, emphasizing temperature and concentration increases. Other researchers, such as Salleh et al. (2020), studied forced convection using Buongiorno's nanofluid theory around a moving needle, discovering that greater needle thickness reduces heat and mass transfer rates; Jamel et al. (2021) assessed MHD mixed convection over nonlinear surfaces, concluding that stronger Soret effects raise the Soret number, while higher magnetic fields lower velocity. Abas et al. (2016) analyzed the numerical behavior of Casson fluid over a stretching sheet, while Ullah et al. (2017) investigated the effects of thermal diffusion and diffusion-thermo on unsteady mixed convection slip flow of Casson fluid over a nonlinear stretching sheet, finding that diffusion-thermo impacts temperature more than thermal diffusion. Rawi et al. (2017) noted that increasing the composite volume in fluid enhances the temperature profile in Casson fluid. Second-grade (viscoelastic) fluids like silicone exhibit both viscous and elastic properties, and scientists such as Raju and Sandeep (2017), Samrat et al. (2019), and Zuhra et al. (2018) have analyzed Casson fluids with nanoparticles for industrial use. The existing literature also covers fluid dynamics studies across various scientific and engineering fields (Seth et al., 2019; Muhammad et al., 2020). Bhattacharyya (2013) investigated the boundary layer flow of Casson fluid over a stretching or shrinking sheet, highlighting the importance of heat transfer rates on product quality. Bhattacharyya et al. (2013) further examined boundary layer flow with magnetic field effects. Hussanan et al. (2014), using Laplace transforms, explained heat transfer in time-dependent Casson fluid flow. Malik et al. (2014) studied heat transfer on a stretched cylinder with nanoparticles. Hayat et al. (2015) looked into heat sources/sinks and chemical reactions in non-Newtonian Casson fluid flow. Makanda et al. (2015) analyzed hydromagnetic free convection and radiation in viscous dissipative Casson fluids within non-Darcian porous media. Other researchers like Kataria and Patal (2016) and Ahmed (2017) examined various boundary conditions affecting hydromagnetic Casson fluid flows.

ISSN No. 2454-6194 | DOI: 10.51584/IJRIAS |Volume XI Issue I January 2026

Despite the extensive studies mentioned above, no investigation has been conducted on Casson fluid flow with magnetized stretching surfaces, including radiation and chemical reactions. The magnetization of the plate with radiation affects the boundary layer thickness past a steady stretching magnetized sheet, which has not been addressed in the literature. To fill this gap, the current study focuses on steady, incompressible flow of Casson fluid over a magnetized sheet. The study applies similarity transformation and the shooting method to solve the modeled momentum, energy, and concentration equations. Finally, the physical characteristics of the relevant parameters are analyzed and presented through tables and graphs.

Model Formulations

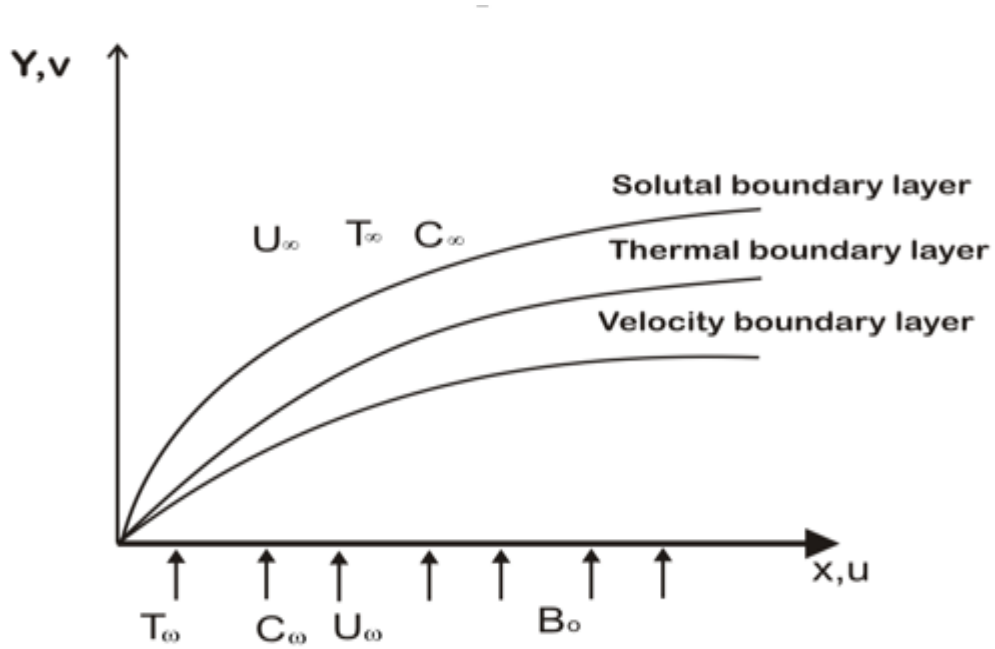

Figure 1: Schematic diagram of magnetized surface

Flow Assumptions for Inclined Magnetized Surface

A steady Casson fluid flowing over a vertically porous and stretched plate at $y,v = 0$, along a transverse magnetic field, is revealed in Figure 3.2. The plate direction is along the x-axis and normal to the y-axis. The fluid is made to occupy half of the space at $y > 0$. The mass transfer and chemical reactions are also retained. In the y-direction of the plate is an applied magnetic field $B_{0,}$ which is constant. A very small Reynolds number is considered so that the induced magnetic field will be less compared to the applied magnetic field. The tangential velocity u_w, due to the stretched surface, is made to vary proportionally to the distance x so that $u_w = ax^n$, where a is the constant.

The rheological equation of state for the anisotropic flow of a Casson fluid can be expressed as (Shehzad *et al*. 2013**):**

$$\begin{cases} 2\left(\mu_B + \dfrac{P_y}{\sqrt{2\pi}}\right) e_{ij}, \mu > \pi_c, \\ 2\left(\mu_B + \dfrac{P_y}{\sqrt{2\pi}}\right) e_{ij}, \mu < \pi_c, \end{cases} \qquad (*)$$

In Equation (3.44), the $(i, j)^{th}$ component deformation rates are $\pi = e_{ij}e_{ij}$ and $e_{ij.}$ The π is the product of the component of deformation rate with itself, π_c is the critical value of this product based on the non-Newtonian model, and μ_B is the fluid's plastic dynamic viscosity of the Newtonian model. Fluid and P_y is the yield stress of the fluid.

The mathematical models are derived from the established Casson model.

ISSN No. 2454-6194 | DOI: 10.51584/IJRIAS |Volume XI Issue I January 2026

Casson modelled the viscosity in his equation in the form $(1 + 1/\beta)^{\omega}$ where β is the Casson parameter. The new model for the viscosity for Casson-like fluids, known as the Casson fluid, is modified to give;

$$\mathcal{V} = \left(1 + \frac{1}{\beta}\right)^{\frac{2}{3}} \mathcal{V} \qquad (1)$$

Where β is the Casson parameter, and ω is the order parameter. For Casson fluid, ω = 1. However, if ω is not one (1), then ω could take the value of odd, even, or a fraction. The omega (ω), taking any of these values, will produce another type of fluid Casson fluid. This type of fluid also has similar characteristics to Casson and other non-Newtonian fluids.

Assuming ω to be a fraction, then the viscosity will be modified as:

$$\mathcal{V} = \mathcal{V} \sqrt[3]{\left(1 + \frac{1}{\beta}\right)^2} \qquad (2)$$

Let us consider a dissipative steady Casson fluid flow on a stretching magnetized plate that co-occurs with the plate at y = 0. Assuming the fluid flow is restricted to y > 0 with two equal but opposite forces acting along the horizontal (x-axis), so that the sheet is stretched to keep the origin rigid, is shown in Figure 1. Supposing the velocities along the x and y axes are respectively represented by u and v, with T being the temperature and C, the concentration of the fluid, then the governing models of the steady Casson fluid can be obtained from.

$$\frac{\partial u}{\partial x} + \frac{\partial v}{\partial y} = 0 \qquad (3)$$

$$u\frac{\partial u}{\partial x} + v\frac{\partial u}{\partial y} = \mathcal{V} \sqrt[3]{\left(1 + \frac{1}{\beta}\right)^2} \frac{\partial^2 u}{\partial y^2} + \beta_T (T - T_\infty) + \beta_C (C - C_\infty) \qquad (4)$$

$$\frac{\partial T}{\partial x} + v\frac{\partial T}{\partial y} = \alpha \frac{\partial^2 T}{\partial y^2} + \frac{\mathcal{V}}{c_p} \sqrt[3]{\left(1 + \frac{1}{\beta}\right)^2} \left(\frac{\partial u}{\partial y}\right)^2 - \frac{\alpha}{k}\frac{\partial q_r}{\partial y} \qquad (5)$$

From equation (4), $\frac{\partial q_r}{\partial y}$ can further be simplified as follows;

$$q_r = -\frac{4\sigma^*}{3K'}\frac{\partial T^4}{\partial y} \qquad (6)$$

We assume that the temperature differences within the flow, such as the term T^4, may be expressed as a linear function of temperature. Hence, expanding T^4 in a Taylor series about T_∞ and neglecting higher-order terms, we get;

$$T^4 \cong 4T_\infty{}^3 T - 3T_\infty{}^4 \qquad (7)$$

Multiplying through (6) by $\frac{\partial}{\partial y}$ and ignoring higher terms gives,

$$\frac{\partial T^4}{\partial y} \cong 4T_\infty{}^3 \frac{\partial T}{\partial y} \qquad (8)$$

Equation (7) simplifies:

$$\frac{\partial q_r}{\partial y} = -\frac{4\sigma^*}{3k'} * 4T_\infty{}^3 \frac{\partial T}{\partial y} \qquad (9)$$

ISSN No. 2454-6194 | DOI: 10.51584/IJRIAS |Volume XI Issue I January 2026

Differentiating (8) with respect to *y* gives,

$$\frac{\partial q_r}{\partial y} = -\frac{4\sigma^*}{3k'} * 4T_\infty{}^3 \frac{\partial^2 T}{\partial y^2} \qquad (10)$$

$$\frac{\partial T}{\partial x} + v\frac{\partial T}{\partial y} = \alpha\frac{\partial^2 T}{\partial y^2} + \frac{\mathcal{V}}{c_p}\sqrt[3]{\left(1+\frac{1}{\beta}\right)^2}\left(\frac{\partial u}{\partial y}\right)^2 + \frac{\alpha}{k}\frac{4\sigma^*}{3k'} * 4T_\infty{}^3\frac{\partial^2 T}{\partial y^2} \qquad (11)$$

$$u\frac{\partial C}{\partial x} + v\frac{\partial C}{\partial y} = D\left(\frac{\partial^2 C}{\partial y^2}\right) + \gamma(C - C_\infty) \qquad (12)$$

Boundary Conditions are;

The boundary conditions for the problem are;

$$u = u_w = U_0(B)ax^n, \quad V = V_w, T = T_W, \qquad C = C_W \qquad as\ y = 0 \qquad (13)$$

$$u \to 0, T \to T_\infty\ C \to C_\infty \qquad as\ y \to \infty \qquad (14)$$

Similarity Analysis

Introducing the stream function defined as $\psi = x^n\sqrt{av}f(\eta)$ and a dimensionless variable, $\eta = y\sqrt{\frac{a}{v,}}$ and noting that the velocity components relate to the stream function in the usual way as

$$u = \left(\frac{\partial\psi}{\partial y}\right)_x \text{ and } v = \left(\frac{\partial\psi}{\partial x}\right)_y, \qquad (15)$$

Equation (6) simplifies to;

$$u = ax^n f', v = -\boldsymbol{n}x^{n-1}\sqrt{avx^{n-1}}f, \qquad (16)$$

Equation (2) is satisfied identically by equation (7).

Introducing the similarity variables, $T = T_o\theta + T_\infty, and\ C\ = (C_w - C_\infty)\phi + C_\infty$, equations (3), (4), and (5) transform into;

$$\sqrt[3]{\left(1+\frac{1}{\beta}\right)^2} f''' - nf'^2 + \boldsymbol{n}ff'' + \mathrm{Gr}\theta + \mathrm{Gm}\phi = 0 \qquad (17)$$

$$\left(\mathbf{1} - \frac{4}{3}Ra\right)\boldsymbol{\theta}'' + \boldsymbol{nPrf\theta}' + \boldsymbol{Br}\sqrt[3]{\left(1+\frac{1}{\beta}\right)^2}\boldsymbol{f}''^{\mathbf{2}} + \mathrm{Pr}Q\theta = \mathbf{0} \qquad (\mathbf{18})$$

$$\frac{\mathbf{1}}{\boldsymbol{Sc}}\phi'' + \boldsymbol{nf}\phi' + \boldsymbol{\lambda}\phi = \mathbf{0} \qquad (\mathbf{19})$$

Where the number of times a function is differentiated with respect to η is represented by prime symbol(s). The local Grashof and the modified Grashof numbers, respectively represented by $Gr = \frac{g\beta_t T_0}{a^2 x^{2n-1}}$ and $Gm = \frac{g\beta_C C_0}{a^2 x^{2n-1}}$, $\lambda = \frac{\gamma}{ax^{n-1}}$ is the reaction rate parameter**,** $\mathrm{Pr} = \frac{\upsilon}{\alpha}$ represents the Prandtl number, $\mathrm{Ra} = \frac{4\sigma^* T_\infty^3}{\kappa K'}$ represents the thermal radiation parameter, $Br = PrEc$, but

ISSN No. 2454-6194 | DOI: 10.51584/IJRIAS |Volume XI Issue I January 2026

$Ec = \frac{a^2 x^n}{c_p}$ is the Eckert number, $Q = \frac{\lambda_T}{\rho c \boldsymbol{a x^{n-1}}}$ is the heat source dimensionless parameter, $Sc = \frac{\upsilon}{D}$ is the Schmidt number, and $\sqrt[3]{\left(1+\frac{1}{\beta}\right)^2}$ is the Casson parameter when the order is a fraction.

The convective boundary conditions are;

When y = 0, $u = u_w,\ \eta = 0, v = V_w, C = C_w\ and\ T = T_w$.

Thus, $f'(0) = 1 - M, f(0) = f_w, \theta(0) = 1,\ \phi(0) = 1\ as\ \eta = 0$

$$f'(\infty) = 0, \theta(\infty) = 0, \phi(\infty) = 0\ as\ \eta \to \infty \qquad (20)$$

where $M = \frac{\sigma \overline{B}_0^2}{a\rho/L}$ is the magnetic field at the surface

Numerical Procedure

Equations (10), (11), and (12) represent the coupled ordinary differential equations, while equation (13) defines the corresponding boundary conditions. These coupled ODEs are of third order and, as such, are challenging to solve directly. To simplify the solution process, we apply order reduction techniques by letting;

$$f = x_1, f' = x_2, f'' = x_3,\ \ f''' = x_4,\ \theta = x_5, \theta' = x_6, \phi = x_7,\ \ \phi' = x_8 \qquad (21)$$

Eqs (8), (9), and (10) are then reduced to first-order ODEs as

$$x_1' = x_2 \qquad (22)$$

$$x_2' = x_3 \qquad (23)$$

$$x_3' = \frac{1}{\sqrt[3]{\left(1+\frac{1}{\beta}\right)^2}}(nx_2^2 - n(xx_3) - Grx_5 - Gmx_7) \qquad (24)$$

$$x_5' = \frac{1}{\left(1+\frac{4}{3}Ra\right)}\left(-nPr(x_1x_6) - Br\sqrt[3]{\left(1+\frac{1}{\beta}\right)^2}x_3^2 - PrQx_5\right) \qquad (25)$$

$$x_7' = -Sc(nx_1x_8 + \lambda x_7) \qquad (26)$$

The boundary conditions in (13) become;

$x_2(0) = 1 - M_s, x_1(0) = 0, x_5(0) = 1, x_7(0) = 1$, as η=0

$x_2(\infty) = 0,\ x_5(\infty) = 0, x_7(\infty) = 0$, as $\eta \longrightarrow \infty$ (27)

With the aid of MAPLE – 19 software package, numerical and graphical codes were developed and implemented. A step size of Δh = 0.001 for a convergence criterion of 10^{-6} for all the cases was assumed. The highest value of η_∞ to each parameter was known when the values of the unidentified boundary conditions remained unchanged to a final loop with an error not more than 10^{-6}.

RESULTS AND DISCUSSION

The results of the investigation into the skin friction, denoted by f′(0), and the Nusselt number, represented by −θ′(0), are compared with those of Arthur et al. (2015) and

ISSN No. 2454-6194 | DOI: 10.51584/IJRIAS |Volume XI Issue I January 2026

Salahuddin (2021) for varying values of the Prandtl number, as shown in Table 7. The results exhibit perfect agreement to six decimal places.

Table 1 Comparison of values of $-\theta'(0)$ for different values of Pr.

Pr	Arthur *et al*., (2015)	Salahuddin *et al*.(2021)	Present Study $M_s>0$
1.5	0.591354	0.591354	0.492951
1.7	0.668564	0.668564	0.569908
1.9	1.176445	1.176445	1.065134
2.0	3.231326	3.231326	2.833451

Effects of Parameters on Skin Friction and the Rate of Heat and Mass Transfer

The results of varying parameter values on the local skin friction coefficient, the local Nusselt number and the local Sherwood number, are shown in **Table 2**. It is observed that the skin friction decreases with increasing values of Pr, λ, Ra, β, and fw with increasing values Q, Br, and Sc This means that the effect of high viscosity, thermal diffusion, the Casson parameter and suction at the surface of the sheet, the local skin friction decreases. A higher Prandtl number leads to a thicker velocity boundary layer, which reduces the velocity gradient at the wall, resulting in lower skin friction. Again a higher Prandtl number indicates a lower thermal conductivity, which reduces thermal gradients and consequently, reduces the velocity gradients thereby reducing the skin friction. These combine effects lead to decrease in the local skin friction. The combined effects of the heat sourse, Brinkmann number, and chemical reaction of the fluid collectively contribute to an increase in local skin friction at the plate's surface. Moreover, it is observed that the rate of mass transfer increases with increasing values of Pr, λ, *fw* and Ra; and decreases with increasing values of M.

Table 2. Results of skin friction coefficient [$f''(0)$], Nusselt [$-\theta'(0)$] and Sherwood numbers [$-\phi'(0)$] for various values of controlling parameters.

Pr	λ	Br	Ra	N	β	Sc	Gr	Gm	M	Fw	Q	$f''(0)$	$-\theta'(0)$	$-\phi'(0)$
1.0	0.1	0.1	0.1	1	0.7	0.5	0.1	0.1	0.1	0.1	0.1	-0.376552	-6.639961	0.426168
2.0												-0.521798	-3.234456	0.374175
3.0												-0.563334	-1.625055	0.361749
	0.2											-0.377465	-6.541430	0.359847
	0.3											-0.378702	-6.398319	0.279258
		0.2										-0.375152	-6.711542	0.426557
		0.3										-0.373556	-6.782861	0.426946
			0.2									-0.409950	-6.215859	0.413300
			0.3									-0.453472	5.344798	0.397246
				2.0								-0.726783	0.174228	0.591740
				3.0								-0.872573	0.778369	0.762934
					0.8							-0.378360	-6.838040	0.426442

					0.9							-0.379767	6.997476	0.426684
						0.6						-0.375471	6.776431	0.482522
						0.7						-0.374870	-6.870185	0.534455
							0.2					-0.336286	-3.436570	0.430864
							0.3					-0.296655	-2.357031	0.435366
								0.2				-0.357158	-5.944008	0.427051
								0.3				-0.428032	-5.264108	0.428032
									0.2			-0.232597	-7.680573	0.416130
									0.3			-0.091507	-8.760013	0.406215
										0.2		-0.427150	-5.799135	-0.451016
										0.3		-0.479950	-4.898831	-0.476799
											1.1	-0.307185	-9.684424	0.442119
											1.2	-0.230357	-13.352202	0.457676

Graphical Results

Velocity Profiles

The influence of thermophysical parameters on the velocity field of the non-Newtonian Casson fluid is shown in Figures 2–12. The far-field boundary conditions are satisfied when the velocity at the plate's surface is minimal and gradually increases to the free stream value. The effects of the suction parameter (fw) and the surface magnetic parameter (M) on the velocity profiles are presented in Figures 7 and 4, respectively. The combined effects of M and fw result in a reduced velocity. This is due to the transverse magnetic field inducing a Lorentz force that opposes the fluid's motion, while suction also hinders the flow, thereby decreasing the velocity field near the surface.

The effect of the Casson parameter (β) on the velocity field is shown in Figure 6. It is observed that the Casson parameter negatively impacts the velocity field, as the increased plastic dynamic viscosity creates resistance to the flow. Additionally, the Grashof number, shown in Figure 2, favors buoyancy forces and enhances the flow speed.

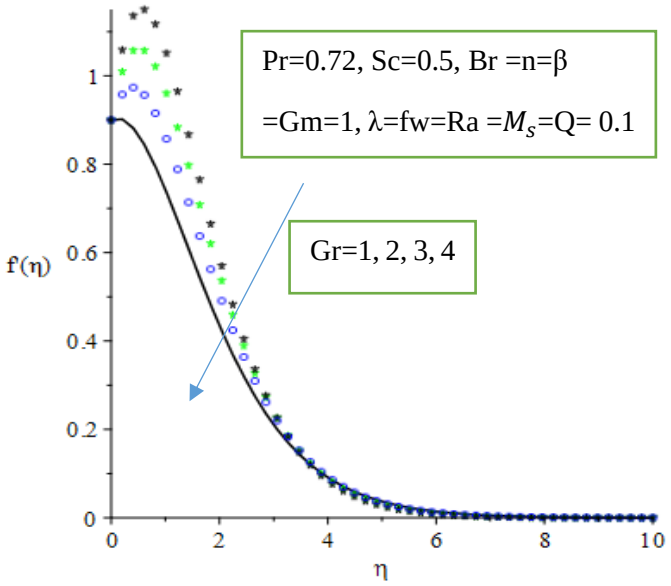

Figure 2: Velocity profiles with varying values of Grashof parameter

ISSN No. 2454-6194 | DOI: 10.51584/IJRIAS |Volume XI Issue I January 2026

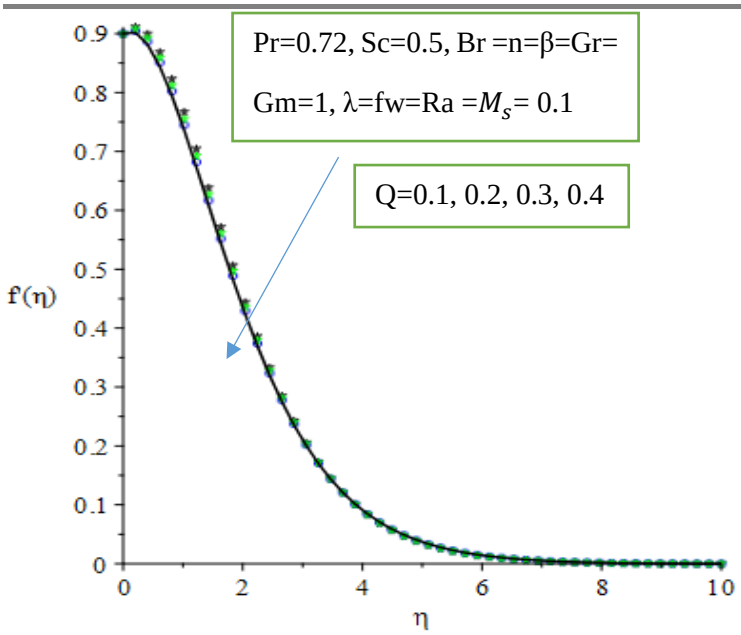

Figure 3: Velocity profiles with varying values of Heat source parameter.

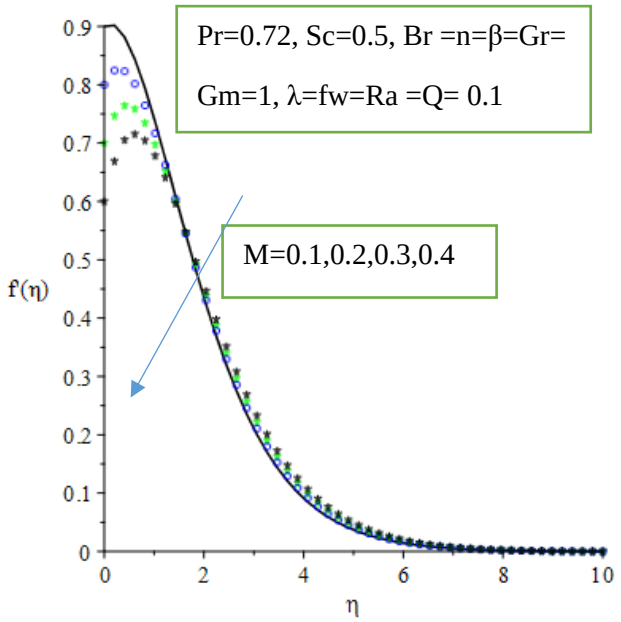

Figure 4: Velocity profiles with varying values of Magnetic parameter

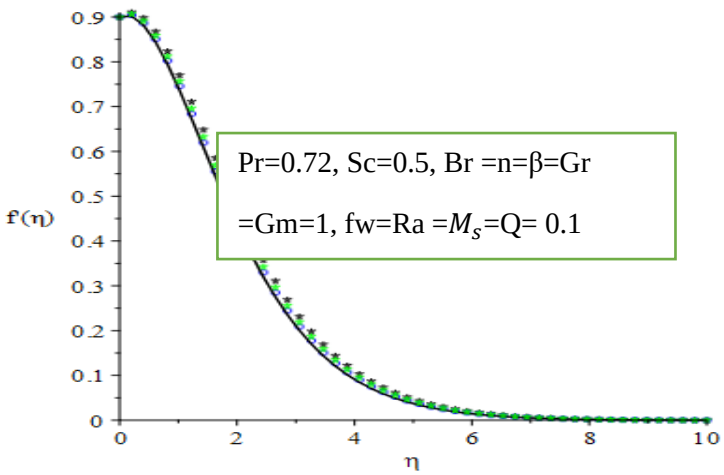

Figure 5: Velocity profiles with varying values of Reaction rate parameter.

ISSN No. 2454-6194 | DOI: 10.51584/IJRIAS |Volume XI Issue I January 2026

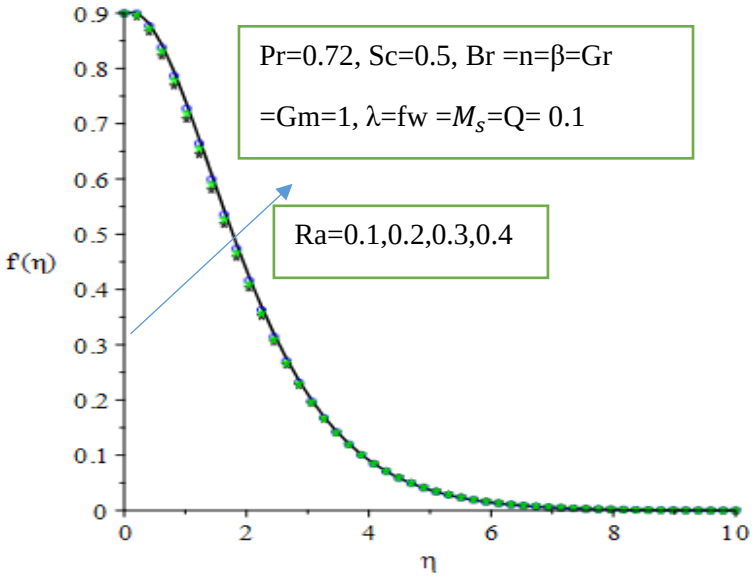

Figure 6: Velocity profiles with varying values of Radiation parameter

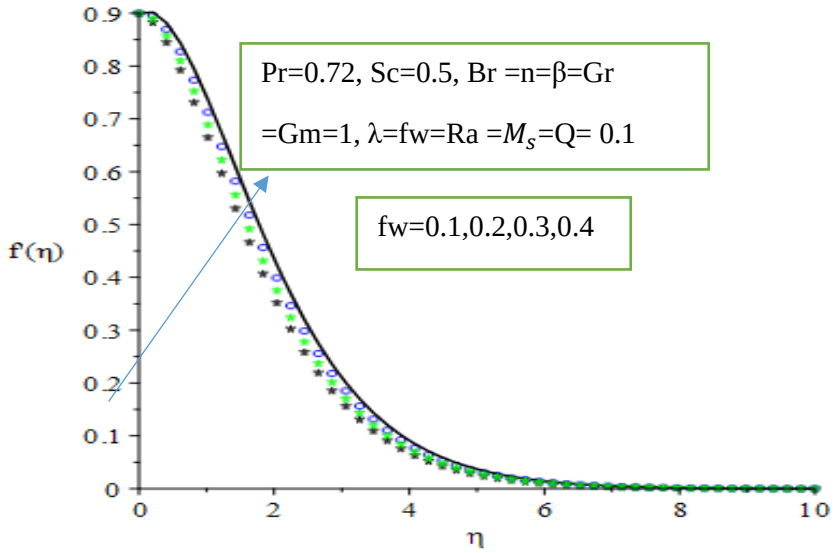

Figure 7: Velocity profiles with varying values of Suction parameter.

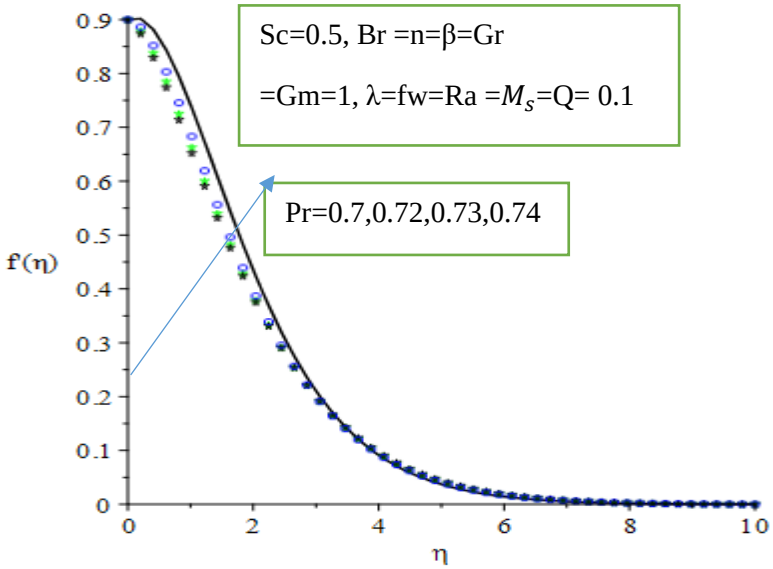

Figure 8: Velocity profiles with varying values of Prandtl parameter

ISSN No. 2454-6194 | DOI: 10.51584/IJRIAS |Volume XI Issue I January 2026

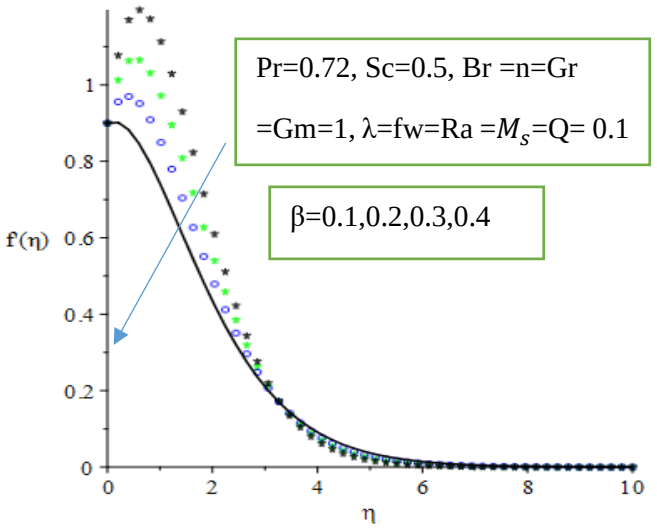

Figure 9: Velocity profiles with varying values of Casson parameter

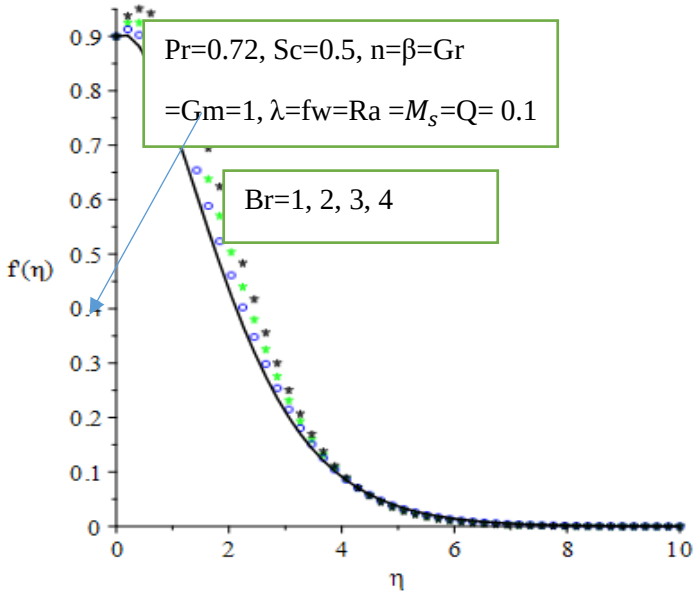

Figure 10: Velocity profiles with varying values of Brinkman parameter

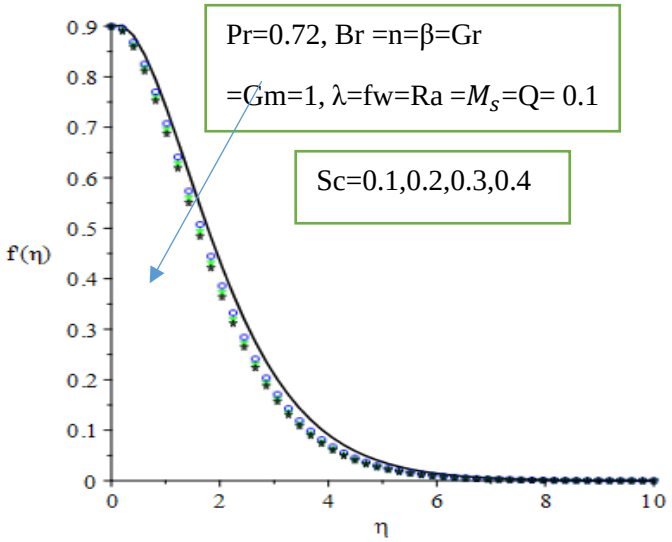

Figure 11: Velocity profiles with varying values of Schmidt parameter.

ISSN No. 2454-6194 | DOI: 10.51584/IJRIAS |Volume XI Issue I January 2026

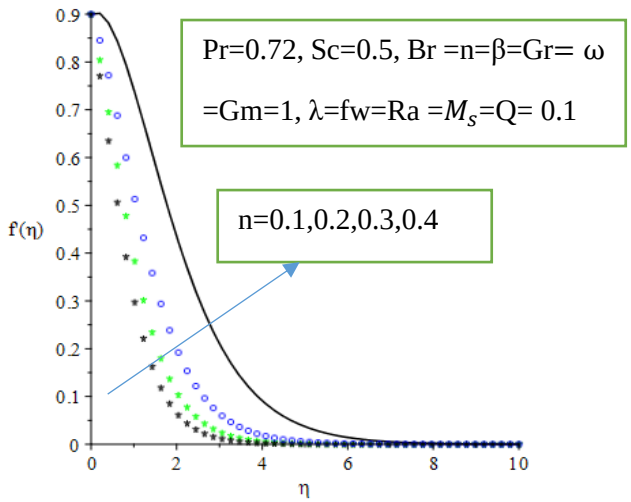

Figure 12: Velocity profiles with varying values of Stretching parameter

Temperature Fields

Figures 13–24 illustrate the effects of parameter variation on the thermal distribution. Figure 14 shows how an increase in the Prandtl number affects the temperature distribution in the fluid. The Prandtl number represents the ratio of momentum diffusivity to thermal diffusivity; higher Prandtl numbers indicate lower thermal diffusivity or higher momentum diffusivity. As a result, increasing the Prandtl number makes convection more responsible for energy transfer than heat diffusion, which reduces the thickness of the thermal boundary layer and leads to faster heat diffusion from the surface.

Figure 13 highlight the effects of magnetic field parameters on the temperature fields. The presence of the magnetic field induces skin-frictional heating, leading to an increase in wall temperature distribution and the thickening of the thermal boundary layer. In Figure 23, it is noted that increasing suction (fw) reduces the temperature distribution on the surface. Figure 21 illustrates the effect of the reaction rate parameter (λ) on the temperature distribution, showing that the thermal boundary layer thickness decreases with an increasing reaction rate parameter. Finally, Figure 18 indicates that thermal radiation (Ra) increases the temperature profiles.

This is because heat generation within the flow leads to an increase in the internal fluid temperature, as indicated by the sharp inclination of the thermal gradient.

The effect of the heat source parameter (Q) on the thermal distribution is shown in Figure 16. It is observed that increasing the heat source parameter (Q) enhances fluid conductivity, which results in the thickening of the thermal boundary layer. Figure 15 illustrates the impact of the viscous dissipation parameter (Br) on the thermal boundary layer. It is noted that increasing the viscous dissipation parameter Br raises the temperature profile, indicating that the temperature distribution improves with increasing viscous dissipation.

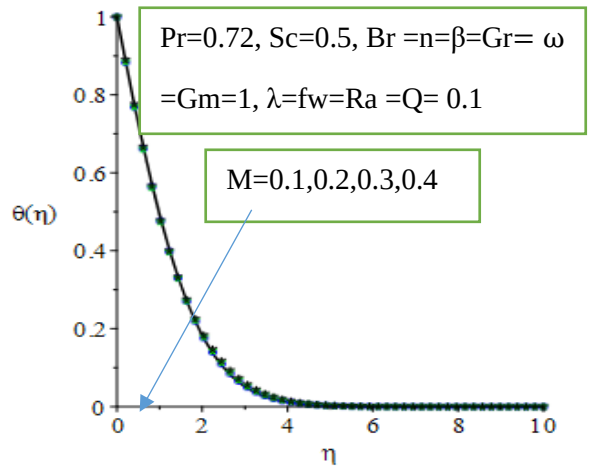

Figure 13: Temperature profiles with varying values of Magnetic parameter

ISSN No. 2454-6194 | DOI: 10.51584/IJRIAS |Volume XI Issue I January 2026

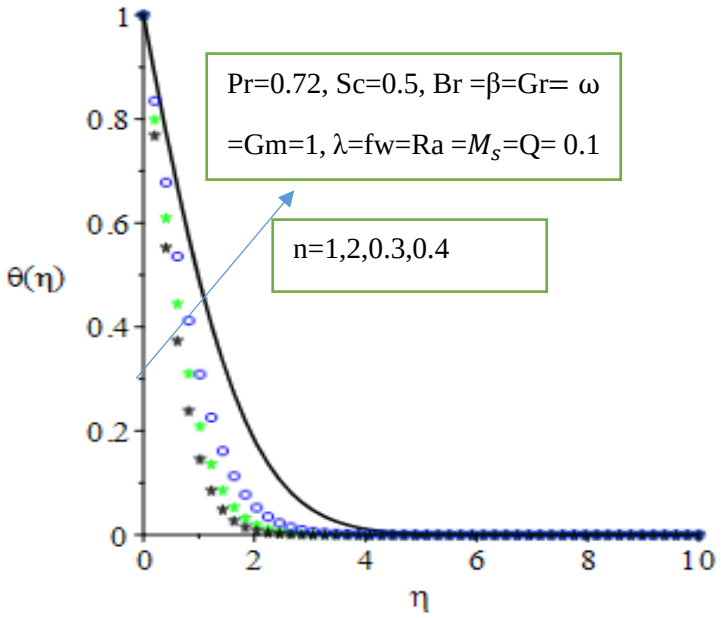

Figure 14: Temperature profiles with varying values of Stretching parameter.

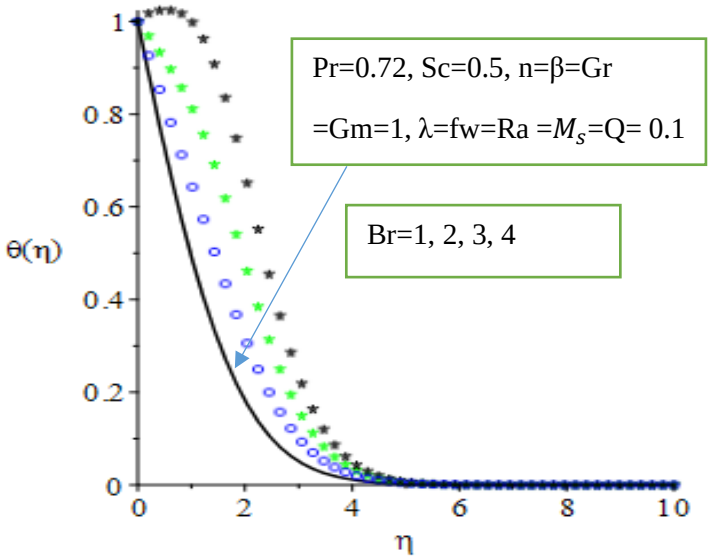

Figure 15: Temperature profiles with varying values of Brinkman parameter

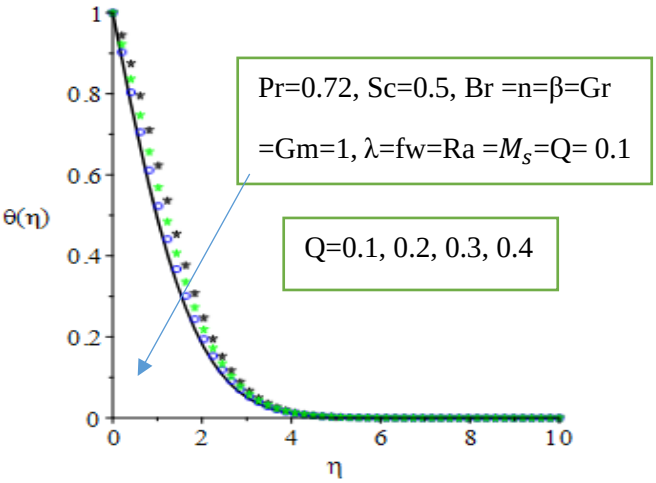

Figure 16: Temperature profiles with varying values of Heat source parameter

ISSN No. 2454-6194 | DOI: 10.51584/IJRIAS |Volume XI Issue I January 2026

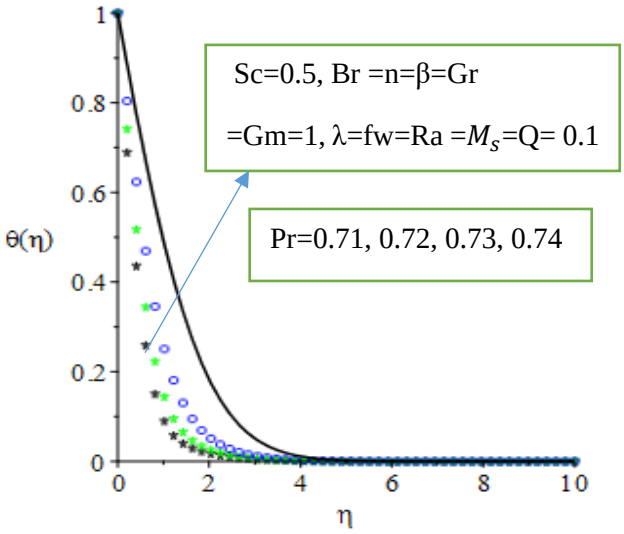

Figure 17: Temperature profiles with varying values of Prandtl parameter

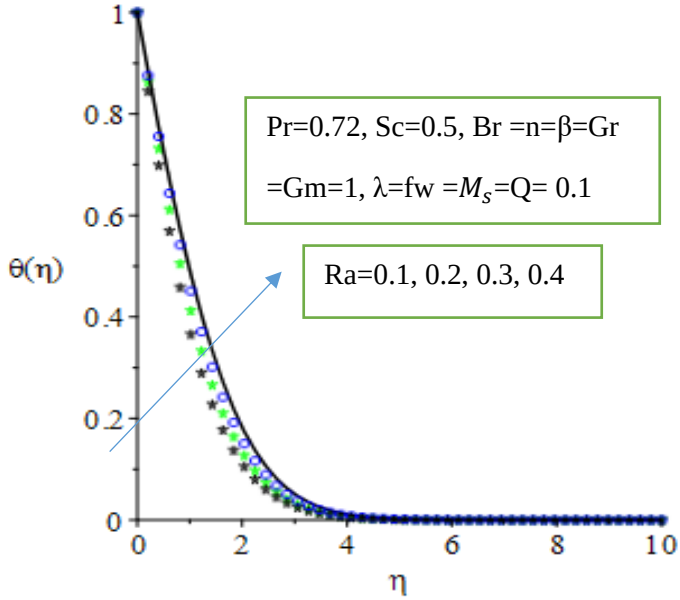

Figure 18: Temperature profiles with varying values of Radiation parameter.

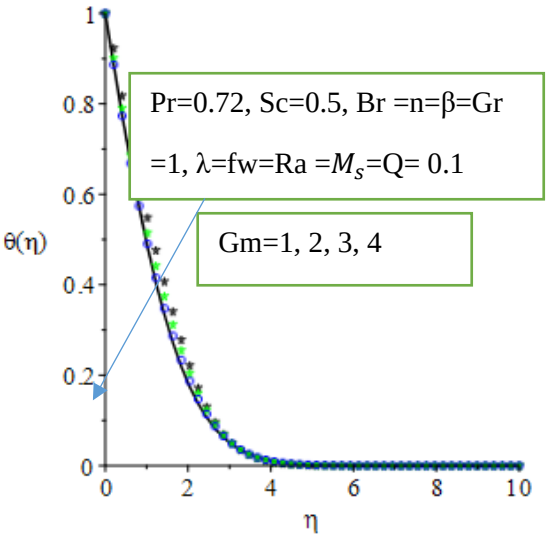

Figure 19: Temperature profiles with varying values of Modified Grashof parameter

ISSN No. 2454-6194 | DOI: 10.51584/IJRIAS |Volume XI Issue I January 2026

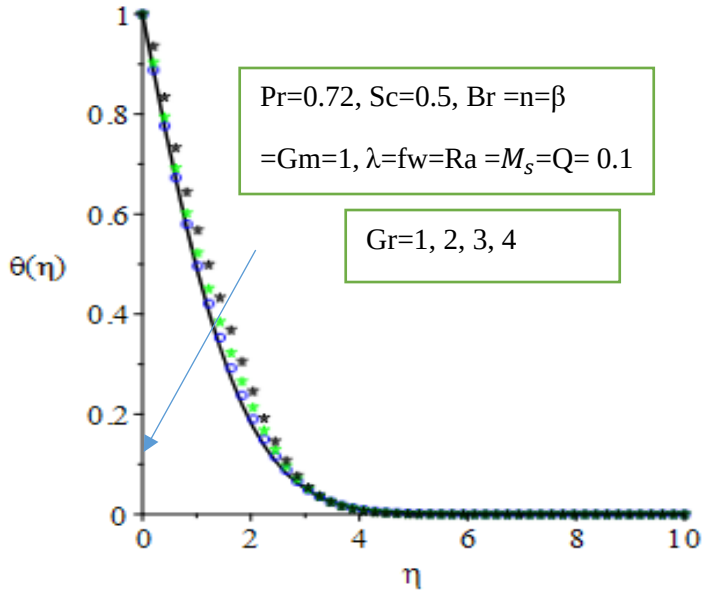

Figure 20: Temperature profiles with varying values of local Grashof parameter

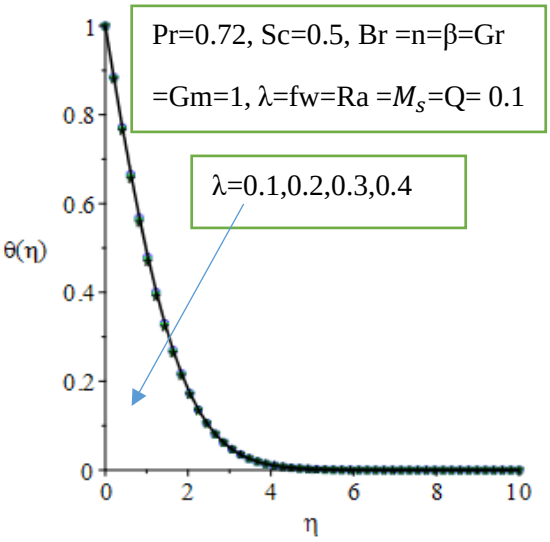

Figure 21: Temperature profiles with varying values of Reaction rate parameter

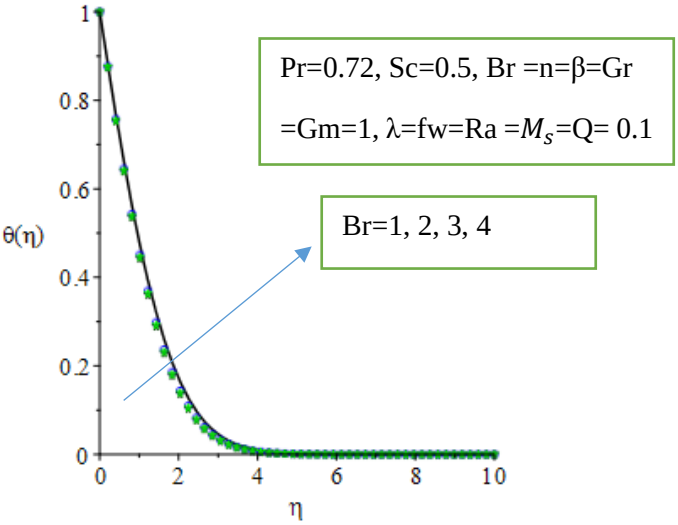

Figure 22: Temperature profiles with varying values of Brinkman parameter.

ISSN No. 2454-6194 | DOI: 10.51584/IJRIAS |Volume XI Issue I January 2026

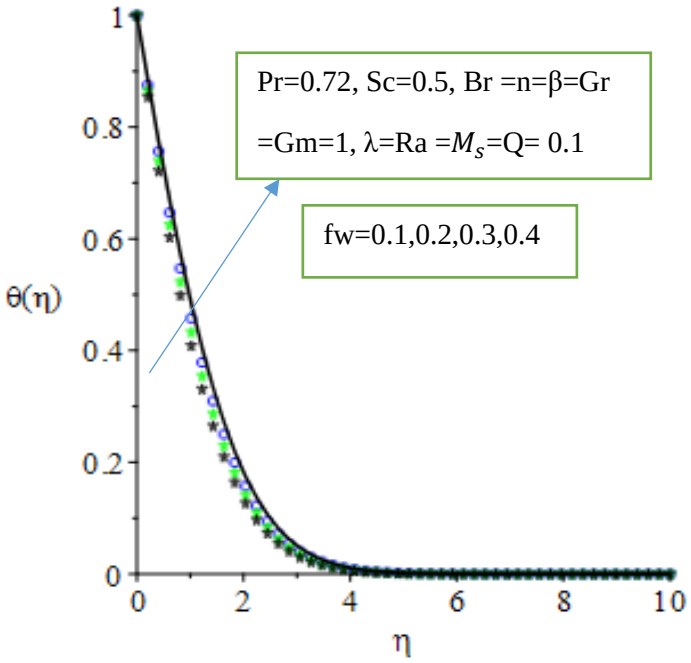

Figure 23: Temperature profiles with varying values of Suction parameter

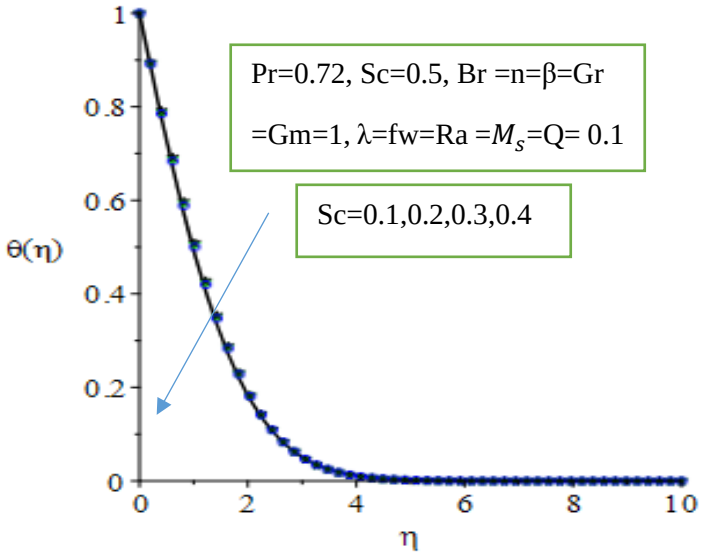

Figure 24: Temperature profiles with varying values of Schmidt parameter

Concentration Profiles

Figures 25–35 illustrate the chemical concentration distribution for non-Newtonian Casson fluid across various thermophysical parameters. The effects of the magnetic parameter (M) is shown in Figures 26. It is noteworthy that increasing the magnetic parameter leads to an increase in the concentration boundary layer thickness. Similarly, the buoyancy force due to species concentration, triggered by an increase in the Grashof number (Gm), reduces the concentration boundary layer thickness, as shown in Figure 31.

Figure 34 confirms that increasing the reaction rate parameter (λ) decreases the concentration of chemical species within the boundary layer. Figure 35 illustrates the effect of the Schmidt number (Sc) on the concentration boundary layer thickness. In practice, increasing the Schmidt number indicates a higher momentum diffusion relative to mass diffusion, which in turn reduces the chemical concentration profile. At a point where λ=0, no chemical reaction occurs. Conversely, increasing the reaction rate parameter (λ) reduces the concentration of

ISSN No. 2454-6194 | DOI: 10.51584/IJRIAS |Volume XI Issue I January 2026

chemical species due to the destructive chemical reaction near the boundary. Figure 29 shows that suction (fw) adversely affects the concentration boundary layer thickness.

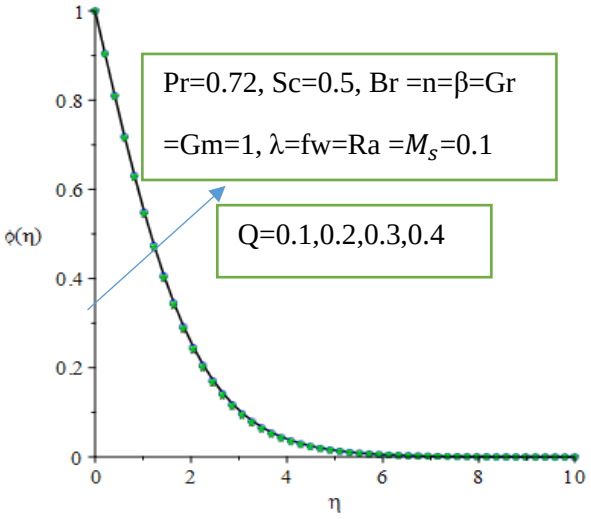

Figure 25: Concentration profiles with varying values of Heat source parameter

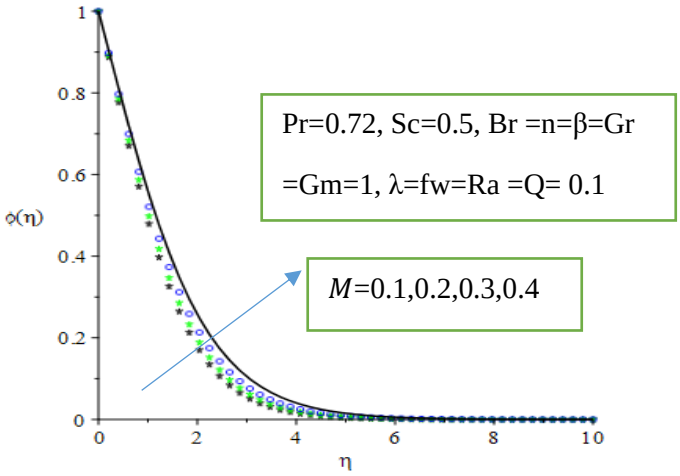

Figure 26: Concentration profiles with varying values of Magnetic parameter.

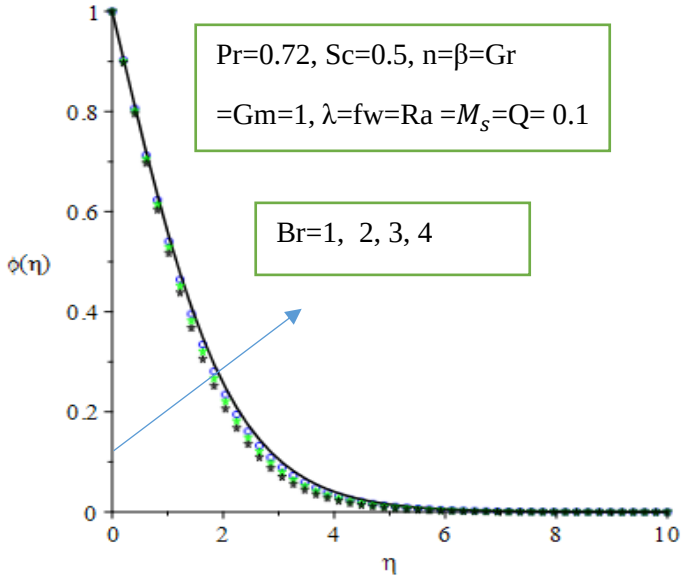

Figure 27: Concentration profiles with varying values of Brinkman parameter

ISSN No. 2454-6194 | DOI: 10.51584/IJRIAS |Volume XI Issue I January 2026

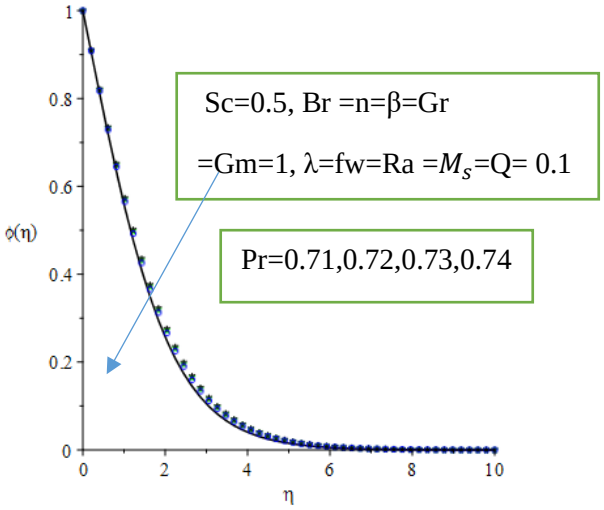

Figure 28: Concentration profiles with varying values of Prandtl parameter.

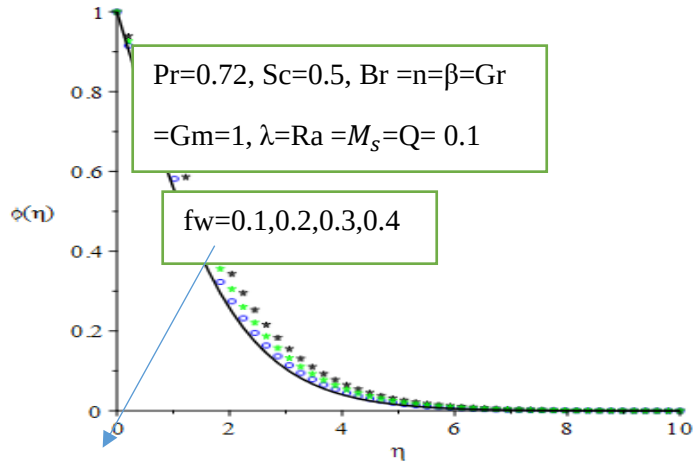

Figure 29: Concentration profiles with varying values of Suction parameter

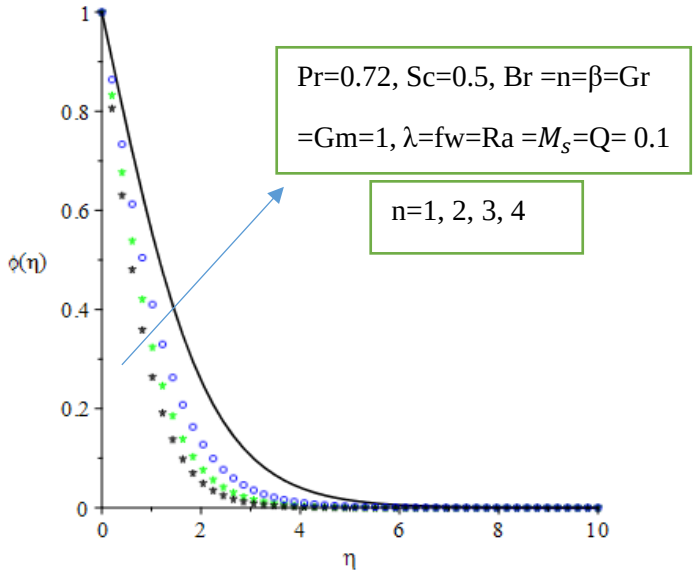

Figure 30: Concentration profiles with varying values of Stretching parameter.

ISSN No. 2454-6194 | DOI: 10.51584/IJRIAS |Volume XI Issue I January 2026

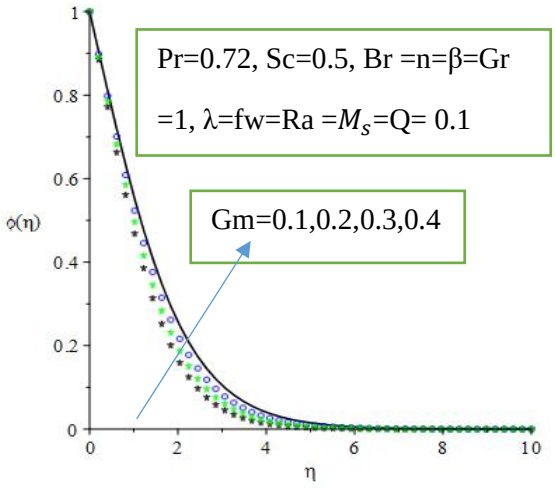

Figure 31: Concentration profiles with varying values of Modified Grashof parameter

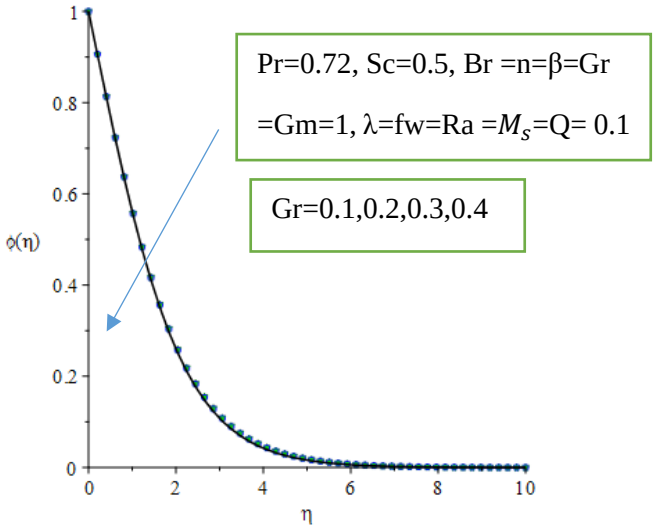

Figure 32: Concentration profiles with varying values of Grashof parameter.

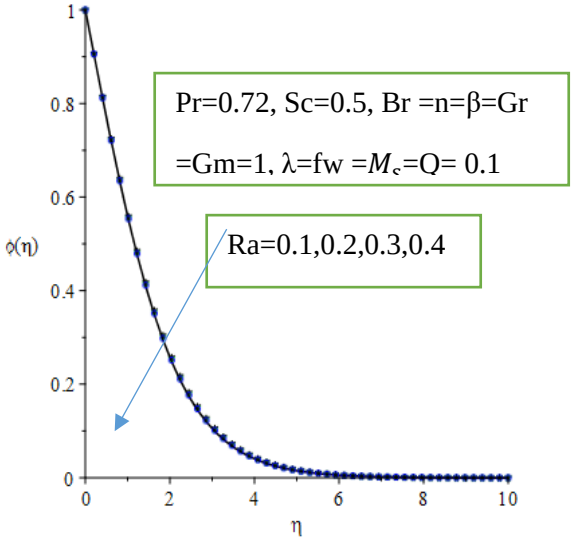

Figure 33: Concentration profiles with varying values of Radiation parameter

ISSN No. 2454-6194 | DOI: 10.51584/IJRIAS |Volume XI Issue I January 2026

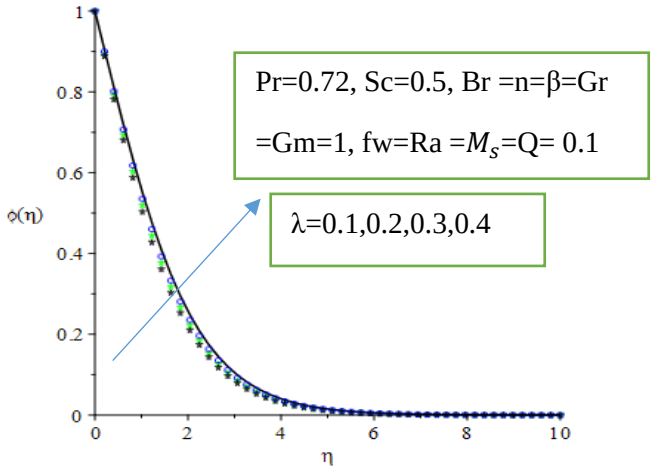

Figure 34: Concentration profiles with varying values of Suction parameter.

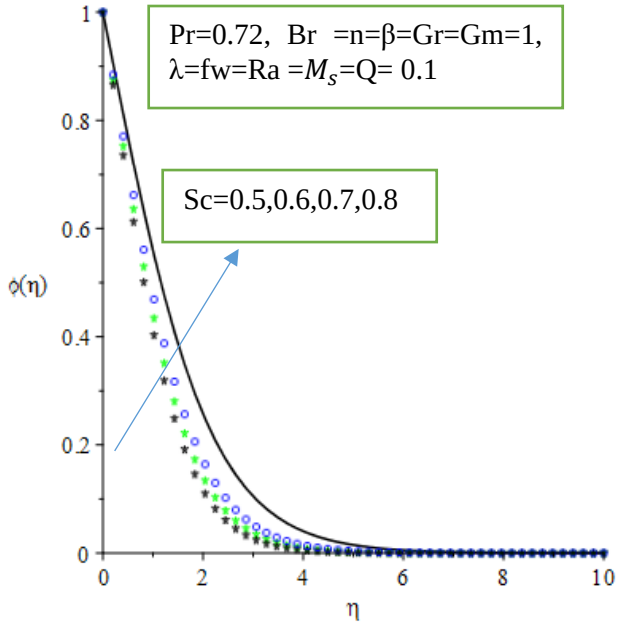

Figure 35: Concentration profiles with varying values of (a) Schmidt parameter

CONCLUSION

This conclusion summarizes the key findings from the research on the mass and thermal energy transfer of Casson fluid on magnetized stretching (or shrinking) sheet under the influence of thermal radiation and suction. Here's a breakdown of the findings:

Fluid Velocity:

The velocity gradient decreases with an increase in the magnetic parameter (M).

The velocity component increases with rising values of M and m.

Fluid Temperature:

The temperature of the fluid increases with the rise in thermal radiation parameter (Ra) and suction parameter (fw).

It decreases as the Prandtl number (Pr) increases.

Concentration of Fluid:

The concentration decreases with the increase in Schmidt number (Sc).

The engineering parameters

1. **Skin Friction Coefficients (Cf):**

The skin friction coefficient in the z-direction (Cf) increases with increasing M

2. **Local Nusselt Number:**

The local Nusselt number decreases with thermal radiation parameter (Ra).

3. **Validation of Results:**

The results obtained in this study are consistent with previously published results, thereby confirming the accuracy of the analytical method employed (Homotopy Analysis Method, HAM).

These findings contribute to a deeper understanding of the hydromagnetic behaviour and thermal-concentration interactions in Carreau fluids, offering valuable insights for industrial applications where such fluids are involved, such as in heat exchangers, polymer processing, and other engineering systems.

Conflict of Interest

The authors declare no financial conflict of interest.

REFERENCES

1. Casson N (1959) In Rheology of Dispersed Systems (Edited by C. C. Mill), Pergamon Press, Oxford, pp. 84.
2. Dash RK, Mehta KN, Jayaraman G (1996) Casson Fluid Flow in a Pipe Filled with a Homogeneous Porous Medium. International Journal of Engineering Science, 34, 1145-1156.
3. Aliseda J, Hopfinger EJ, Lasheras JC, Kreme RDM, Berchieli A, Connolly EK (2008) Atomization of viscous and non-Newtonian liquids by a coaxial, high-speed gas jet. Experiments and droplet size modeling. Int. J. Multipath. Flow 34(2), 161–175.
4. Xiong B, Yang K, Zhao J, Li W, Li K (2008) Performance evaluation of Open Flow-based software-defined networks based on the queueing model, Computer Networks, vol. 102, pp. 172–185, 2016.eld," Chemical Engineering Communications, vol. 195, no. 12, pp. 1575–1584.
5. Seddeek MA (2001) Effects of radiation and variable viscosity on MHD free convection flow past a semi-infinite flat plate with an aligned magnetic field in the case of unsteady flow, International Journal of Heat and Mass Transfer, vol. 45, no. 4, pp. 931–935.
6. Makinde OD (2001) MHD steady flow and heat transfer on the sliding plate, AMSE, Modeling, Measure. Control B, vol. 70, no. 1, pp. 61–70.
7. Makinde OD, Ogulu A (2008) The effect of thermal radiation on the heat and mass transfer flow of a variable viscosity fluid past a vertical porous plate permeated by a transverse magnetic field, Chemical Engineering Communications, vol. 195, no. 12, pp. 1575–1584.
8. Ibrahim SY, Makinde OD (2011) Radiation effect on chemically reacting magnetohydrodynamics (MHD) boundary layer flow of heat and mass transfer through a porous vertical flat plate, International Journal of Physical Sciences, vol. 6, no. 6, pp. 1508–1516, 2011.

9. Sharmila K, Kaleeswari S (2015) Dufour effects on unsteady MHD free convection and mass transfer flow fast through a porous medium in slip regime with heat source/sink. IJSEAS 1(6), 307–320.
10. Arthur EM, Seini IY, Bortteir LB (2015) Analysis of Casson fluid flow over a vertical porous surface with chemical reaction in the presence of the magnetic field. Journal of Applied Mathematics and Physics, 3, 713-723.
11. Mustafa M, Hayat T, Pop I, Aziz A (2011) Unsteady Boundary Layer Flow of a Casson Fluid Due to an Impulsively Started Moving Flat Plate. Heat Transfer-Asian Research, 40, 563-576. http://dx.doi.org/10.1002/htj.20358.
12. El-Aziz MA, Afify AA (2016) Effects of Variable Thermal Conductivity with Thermal Radiation on MHD Flow and Heat Transfer of Casson Liquid Film Over an Unsteady Stretching Surface Brazilian Journal of Physics 46, 516-25.
13. Ishak A, Lok YY, Pop I (2010) Stagnation-Point Flow over a Shrinking Sheet in a Micropolar Fluid. Chemical Engineering Communications, 197,1417-1427. http://dx.doi.org/10.1080/00986441003626169
14. Abbas Z,Sheikh M, Motsa SS (2016) Numerical solution of binary chemical reaction on stagnation point flow of Casson fluid over a stretching/shrinking sheet with thermal radiation Energy 95, 12-20.
15. Ullah I, Khan I, Shafie S (2017) Soret and Dufour effect on unsteady mixed convective slip flow of Casson fluid over a nonlinearly stretching sheet with convective boundary condition. Scientific report, Vol. 7, pp. 11–13 doi:10.1038/s41598-017-01205-5.
16. Rawi NA, Ilias MR, Lim YJ, Isa ZM, Shafie S (2017) Unsteady mixed convection flow of Casson fluid past an inclined stretching sheet in the presence of nanoparticles. In: Journal of Physics: Conference Series.
17. Raju CSK, Sandeep N (2017) Unsteady Casson nanofluid flow over a rotating cone in a rotating frame filled with ferrous nanoparticles: A numerical study Journal of Magnetism and Magnetic Materials 421, 216-24.
18. Samrat SP, Sulochana C, Ashwinkumar GP (2019) Impact of Thermal Radiation on an Unsteady Casson Nanofluid Flow Over a Stretching Surface International Journal of Applied and Computational Mathematics 5.
19. Zuhra S, Khan NS, NS, Islam S (2018) Magnetohydrodynamic second-grade nanofluid flow containing nanoparticles and gyrotactic microorganisms Computational and Applied Mathematics 37, 6332-58.
20. Seth GS, Bhattacharyya A, Kumar R, Mishra MK (2019) Modeling and numerical simulation of hydromagnetic natural convection Casson fluid flow with nth-order chemical reaction and Newtonian heating in a porous medium, J. Porous Media 22 (9).
21. Bhattacharyya K, Hayat T, Alsaedi A (2013a) Exact Solution For Boundary Layer Flow of Casson Fluid over a Permeable Stretching/Shrinking Sheet, Z. Angew. Math. Mech.
22. Hussanan A, Zukhi SM, Tahar RM, Khan I (2014) Unsteady boundary layer flow and heat and mass transfer of a Casson fluid past an oscillating vertical plate with Newtonian heating. PLOS ONE, 9: e108763. https://doi.org/10.1371/journal.pone.0108763
23. Malik MY, Naseer M, Nadeem S, Rehman A (2014) The boundary layer flow of Casson nanofluid over a vertical exponentially stretching cylinder. Applied Nanoscience, 4: 869-873. https://doi.org/10.1007/s13204-013-0267-0
24. Hayat T, Bilal AM, Shehzad SA, Alsaedi A (2015) Mixed convection flow of Casson nanofluid over a stretching sheet with convectively heated chemical reaction and heat source/sink. Journal of Applied Fluid Mechanics, 8, 803-811. https://doi.org/10.18869/acadpub.jafm.67.223.22995
25. Makanda G, Shaw S, Sibanda P (2015) Effects of radiation on MHD free convection of a Casson fluid from a horizontal circular cylinder with partial slip in nonDarcy porous medium with viscous dissipation. Boundary Value Problems, 2015: 75. https://doi.org/10.1186/s13661-015-0333-5
26. Kataria HR, Patal HR (2016) Soret and heat generation effects on MHD Casson fluid flow past an oscillating vertical plate embedded in a porous medium. Alexandria Engineering Journal, 55: 2125-2137. https://doi.org/10.1016/j.aej.2016.06.024
27. Ahmed A (2017) The influence of slip boundary condition on Casson nanofluid flow over a stretching sheet in the presence of viscous dissipation and chemical reaction. Hindawi, 2017: 1-12. https://doi.org/10.1155/2017/3804751

28. Chenna DK, Seshagiri RYV, Satheesh YKR, Vishnuvardhan V, Raju D (2025) Chemical Reaction and Soret Effects on MHD Free Convection Flow Past an Accelerated Vertical Plate Through a Porous Medium with Heat Source. International Journal of Food and Nutritional Sciences, 11(12), 165–183.
29. Yahaya SD, Faisal S (2018) Impact of thermal radiation on electrical MHD flow of nanofluid over a nonlinear stretching sheet with variable thickness. Alexandria Engineering Journal. 57, pp 2187-2197
30. Chenna DK, Nagaraju V, Bhumarapu V (2023) Investigating the Influence of Chemical Reaction on MHD-Casson Nanofluid Flow via a Porous Stretching Sheet with Suction/Injection. Science, Engineering and Technology, 3(2), 47–62.
31. Gireesha BJ, Kumar KG, Krishnamurthy MR, Manjunatha S, Rudraswamy NG (2019) Impact of Ohmic heating on MHD mixed convection flow of Casson fluid by considering cross diffusion effect. **Journal** Nonlinear Engineering, 8(1), 380-388, https://doi.org//10.1515/nteng-2017-0144.
32. Gbadeyan JA, Oyekunle TL, Fasogbon PE, Abubakar JU (2018) Soret And Dufour Effects On Heat And Mass Transfer In Chemically Reacting MHD Flow Through A Wavy Channel. Journal of Taibah University for Science. 12(5), pp 631-651
33. Oreyeni T, Omokhuale E (2019) Optimal Homotopy Analysis of MHD Natural Convection Flow of Thixotropic Fluid under Subjection of Thermal Stratification: Boundary Layer Analysis. American Journal of Computational Mathematics, **9**, 116-131. doi: 10.4236/ajcm. 2019.92009.
34. Rasool G, Shafiq A, Baleanu D (2020) Consequences of Soret-Dufour effects on thermal radiation, and binary chemical reaction on Darcy-Forchheimer flow of Nanofluids. Symmetry. 12, pp 1421. doi:10.33/sym12091421
35. Salleh SNA, Bachok N, Araifin NM, Ali FM (2020) Influence of Soret and Dufour on forced convection flow towards a moving thin needle considering Buongiorno's nanofluid model. Alexandria Engineering Journal. 59(5), pp 3897-3906 http://doi.org/10.1016/j.aes.2020.06.045.
36. Jamel B, Abdelhafez MA, Abd-Alla, AM, Abo-Dahab SM, Mahmot KH (2021) MHD mixed convection Nanafluid flow over a convectively heated nonlinear surface due to an extending surface with Soret Effect. Complexity; Hohken Vol 2021.Doi:10.1155/2021/5592024

ISSN No. 2454-6194 | DOI: 10.51584/IJRIAS |Volume XI Issue I January 2026

NOMENCLATURE

u, v, w Velocity	components along x, y and z axes (m/s)		q_r	Radiation flux distribution in fluid (W/m^2)
B_0	Applied magnetic field (Wb/ m^2)		Nu	Nusselt number
t	Time (s)		Sh	Sherwood number
T_w	Wall temperature (K)		K	Thermal conductivity of the fluid (W/m/K)
U_0	Characteristic velocity (m/s)		Pr	Prandtl number
C	Concentration (kg/m^3)		$q^{\cdot}$	Volumetric heat generation
g	Acceleration due to gravity (m/s^2)		M	The magnetic parameter at the surface
T	Temperature of the Casson fluid (K)		Br	The Brinkmann parameter
η	Similarity variable		$\theta(\eta)$	Dimensionless temperature
$f(\eta)$	Similarity function			
Greek symbols				
β	Casson parameter		P	Fluid density
η	Similarity variable		Λ	Internal heat generation parameter
σ	Electrical conductivity of the base fluid (m^2/s)		α	Thermal diffusivity
ω	Casson fluid order		N	Kinematic viscosity (m^2/s)
$\boldsymbol{\psi}$	Stream function, (m^2 /s)		μ	Fluid viscosity (kg/m/s)

ISSN No. 2454-6194 | DOI: 10.51584/IJRIAS |Volume XI Issue I January 2026

β_T	The thermal coefficients (1/K)		β_C	Concentration expansion coefficients (1/kgm^3)